Fibre behaviour in the spunbonding process. Part II: Modelling fibre dynamics in the diffuser

Journal:	*Part C: Journal of Mechanical Engineering Science*
Manuscript ID:	JMES-15-0239.R1
Manuscript Type:	Original article
Date Submitted by the Author:	20-Jul-2015
Complete List of Authors:	Battocchio, Francesco; University of Cambridge, Engineering Sutcliffe, Michael; University of Cambridge, Engineering
Keywords:	Aerodynamics, Applied Mechanics, Dynamics, Modelling, Polymers, Textile Technology
Abstract:	The behaviour of a fibre subject to the turbulent air flow in the diffuser in the spunbonding process is studied using a three-dimensional dynamics model in which the fibre is discretised as a chain of beads connected by linear and rotational springs. The turbulent air drag acting on the fibre is modelled as a random force, as a function of the mean air velocity, the turbulence intensity, and the spectrum of turbulence. The effect of the air flow parameters and the fibre diameter on the amplitude and the frequency of the fibre oscillations is analysed to understand how the fibre position at the exit of the diffuser is controlled by the turbulent air flow in spunbonding. This in turn will affect fibre laydown and the associated web formation.

Journal Title
XX(X):1–9

DOI: 10.1177/ToBeAssigned
www.sagepub.com/
SAGE

Fibre behaviour in the spunbonding process. Part II: Modelling fibre dynamics in turbulent flows

Francesco Battocchio[1], M. P. F. Sutcliffe[1] and F. Teschner[2]

Abstract

The behaviour of a fibre subject to a turbulent air flow in the spunbonding process is studied using a three-dimensional dynamics model in which the fibre is discretised as a chain of beads connected by linear and rotational springs. The turbulent air drag acting on the fibre is modelled as a random force, as a function of the mean air velocity, the turbulence intensity, and the spectrum of turbulence. The effect of the air flow parameters and the fibre diameter on the amplitude and the frequency of the fibre oscillations is analysed to understand how the fibre laydown and web formation is controlled by the turbulent air flow in spunbonding.

Keywords

spunbonding, nonwovens, fibre dynamics, bead model, turbulence, air drag

Introduction

Overview

The spunbonding process is a widely used industrial technique for the production of nonwoven fabrics, which combines fibre spinning, web formation, and fibre bonding in the same process[1;2]. Material properties such as density, uniformity, stiffness, strength and anisotropy arise, during the fibre web deposition, from the dynamic interaction of the fibres with a turbulent air stream.

In the companion paper, Part I[3], we measured the turbulent air flow in the diffuser of a spunbonding industrial rig, as well as the amplitude of oscillation of a filament with diameter 200 μm and a spun-bonding fibre with diameter 18 μm. It was found that the turbulent air flow can be characterised as a function of the mean and fluctuating air velocity, the energy spectrum, and the length scale of turbulence. It was observed also that a thicker filament oscillates with an amplitude which is larger than that of a thinner fibre, and that the amplitude of fibre motion increases with the air flow rate in the diffuser.

Studying fibre-turbulent air flow interaction is crucial to understanding how fibres move during the laydown and how this feature can influence the fibre orientation and uniformity in the nonwoven web. In this paper we present a mathematical model for the fibre dynamics that allows prediction the amplitude and frequency of fibre motion under a turbulent flow, starting from the air flow parameters measured in Part I. The role of the individual parameters on the fibre motion is investigated and compared with the data measured in the companion paper, Part I.

Fibre dynamics modelling

Despite the large amount of experimental and modelling work that describes fibre spinning in nonwovens[2;4;5], it is not well established how the fibre motion in a turbulent air flow can influence the development of the random fibre web.

Several fibre models exist that study the dynamics of short fibres suspended in shear flow at low Reynolds number. Yamamoto and Matsuoka[6] developed the bead-chain model where the fibre is modelled as a chain of spheres able to stretch, bend, and twist, through varying the distance and the bonding angle between two adjacent spheres. Although this is considered the most comprehensive model for the dynamics of a flexible fibre, the high computational time of $O(N^3)$[7] limits its application only to fibres with small axial ratios, defined as the ratio of the fibre length to the fibre diameter.

The computational time is reduced when fewer elongated bodies are used in place of indiviual spheres. Ross[8] modelled the fibre as made of 20 spheroids, with aspect ratio of 1.25, connected through ball and socket joints, while Nyland[7] used a needle-chain model. Wang[9] developed a rod-chain model in which a flexible fibre is composed of a chain of rigid rods formed by a series of aligned spheres. Although, rod-chain-like models have a lower computational requirement compared to that of the bead-chain models, their CPU time, of the order of $O(N^2)$[9], is still too high for such models to be applied to long fibres. In addition, Xiang[10] reports that their rod-chain code converged only for fibre aspect ratio smaller than 80.

The simulation time of a rigid bodies model can be further decreased to $O(N)$ if a reduced coordinate formulation is used to describe the joint constraints. Hadap[11] applied this method to model the dynamics of hair strands as a rigid multibody chain, for application in hair animations, and solved the rigid body dynamics using Featherstone's

[1]Department of Engineering, University of Cambridge,UK
[2]Fitesa GmbH, Germany

Corresponding author:
Francesco Battocchio, Department of Engineering, University of Cambridge, Trumpigton Street, Cambridge, CB2 1PZ, UK.
Email: francesco.battocchio@gmail.com

Articulated-Body Algorithm[12]. However, Featherstone[13] reports, that for an unbranched chain, the inertia matrix of the system is ill-conditioned, and the solution is affected by problems of accuracy and stability that become more significant as the number of bodies in the chain grows. For a fibre the situation is even worse because of the oscillatory force resulting from the turbulent flow, and the low inertia of the fibre, which require very small time steps. As a result, a large error in the solution is accumulated and the simulation becomes unstable very quickly.

Shambaugh et al. developed a model that predicts the fibre formation and vibration in the melt-blowing process[14;15] in which the mass is concentrated in beads which are subject to an air drag force and a surface tension. This model cannot be directly used to study the dynamics of solidified fibres as the elasticity of the fibre was not considered. Recently a similar fibre formulation was used to understand the whipping motion of microfibres in electrospinning[16].

In this work we develop a fibre bead model that describes the motion of fibres in a turbulent air flow, and we study how the air flow parameters that were measured in Part I influence the behaviour of a fibre in the spun-bonding process. Compared to existing fibre bead models, the elasticity of the fibre is here included for both tensile and bending deformation, and the air drag produced by a turbulent flow is modelled as a function of the mean velocity, the energy of turbulence and the turbulent length scale. In Section 2 an air drag formulation for the fibre-turbulent air flow interaction is presented, Section 3 describes the mathematical formulation of the fibre dynamic model, in Section 4 the accuracy of the fibre model is investigated, and Section 5 the model is used to obtain the amplitude and frequency of the fibre and motion under different air flows and fibre parameters. This is crucial to understand how the fibre deposition and the nonwoven web properties can be influenced by different turbulent air flow regimes.

Air drag model

Fibre air drag

Fibres are spun by an high-speed air flow that applies a skin friction load and stretches the fibres to the final diameter. Sakiadis[17] studied the air drag on a cylindrical surface moving at constant velocity in a fluid using boundary layer theory to find an expression for the skin friction force. Although his prediction matched the results of experiments conducted in laminar flows, the theory poorly estimated the drag on a filament in melt spinning because of the turbulence in the air flow. Later, Matsui[18] solved the problem in terms of the Reynolds Averaged Navier Stokes (RANS) equation along the radial direction of the cylinder, approximating the Reynolds stress with Prandtl theory for the turbulent mixing length. He found that the skin friction force per unit length is:

$$f_f = \frac{1}{2}\pi\, d\rho_a\, C_f\, U^2 \tag{1}$$

where U is the relative velocity fibre-air stream, d is the fibre diameter, ρ_a the density of air, and C_f is a friction coefficient which is a function of the local Reynolds number $\mathrm{Re}_d = Ud/\nu$ as

$$C_f = \beta \mathrm{Re}_d^{-0.61} \tag{2}$$

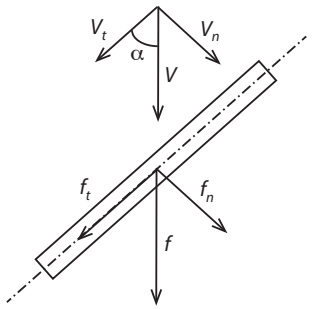

Figure 1. Air drag on a fibre oriented at an angle tilted to the air stream

where β is a constant that depends on the experimental conditions[20].

Ju and Shambaugh[19] obtained empirical relations for the air drag force on a fibre tilted with respect to the air stream, along the direction tangent and normal to the fibre axis. In this study different fibres were tested with a diameter that ranged from 13 μm to 390 μm. They found that, if V_t is the tangential component and V_n is the component normal to the fibre axis, as shown in Figure 1, the tangential air drag f_t is still the friction force given by Equations 1-2 (with V_t in place of U), while the normal force per unit length is

$$f_n = \frac{1}{2}\, d\rho_a\, C_n\, V_n^2 \tag{3}$$

with a normal drag coefficient C_n

$$C_n = A\, \mathrm{Re}_n^{-b} \left(\frac{d}{d_0}\right)^c \tag{4}$$

where, for $d = 13 - 390$ μm, $A = 6.96$, $b = 0.440$, $c = 0.404$, d_0=78 μm, the normal Reynolds number is $\mathrm{Re}_n = V_n d/\nu$, with the viscosity of air $\nu = 1.51 \cdot 10^{-5}$ m^2/s.

Fibre-turbulent flow interaction

In a turbulent flow the velocity of the fluid varies in time and space in a non-deterministic way. An example of the velocity history of a turbulent flow is shown in Figure 2. As in random data analysis[21], also here it is convenient to split the flow velocity vector $\boldsymbol{U}(t, \boldsymbol{r})$ into a mean and a fluctuating component

$$\boldsymbol{U}(t, \boldsymbol{r}) = \overline{\boldsymbol{U}}(\boldsymbol{r}) + \boldsymbol{u}'(t, \boldsymbol{r}) \tag{5}$$

where $\overline{\boldsymbol{U}}(\boldsymbol{r})$ is the time average of $\boldsymbol{U}(t, \boldsymbol{r})$ and $\boldsymbol{u}'(t, \boldsymbol{r})$ is a random fluctuation, assumed isotropic in space. $\boldsymbol{u}'$ is characterized by the root mean square (rms) of U and by the energy spectrum of the random process.

A fully deterministic investigation of the fibre-turbulent flow interaction needs to account for all the turbulence time and length scales associated with the turbulent eddies. Unfortunately this approach is not feasible because it requires geometric meshes and time steps that are computationally too expensive. A reasonable approximation is to consider only the energy containing range of the energy spectrum[22] at low frequency, which is related to the large-scale eddies. Figure 3 shows the energy spectrum measured in Part I of this paper in a spunbonding diffuser at a distance

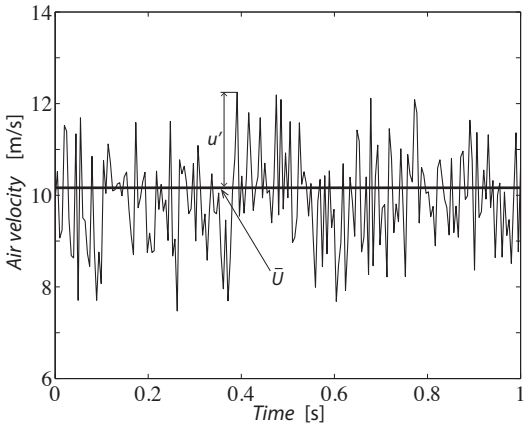

Figure 2. Example of measured air velocity history for a turbulent air flow with mean velocity $\overline{U}$= 10 m/s and fluctuating velocity $u'(t)$.

along the axis of $x = 350$ mm. It can be observed that most of the energy is contained at the lowest frequencies in the highlighted constant region, associated with the largest turbulence scales.

If the energy spectrum $E(\omega)$ is known, a random signal can be simulated as a sum of harmonic functions whose amplitude is derived from the energy spectrum, and random lag phase ϕ_n uniformly distributed in the interval $[0,\, 2\pi]$ [21]. In this study the fluctuating air velocity $u'(t)$ is reproduced using [23]:

$$u(t) = \sqrt{2} \sum_{n=0}^{N-1} A_n \cos(\omega_n t + \phi_n) \qquad n = 0, 1, \ldots, N \tag{6}$$

The amplitude of each harmonic component A_n is obtained from the energy spectrum as:

$$A_n = \sqrt{2\, E(\omega_n) \Delta\omega} \tag{7}$$

where $\Delta\omega$ is calculated from the cut-off frequency ω_c and the total number of harmonics N as $\Delta\omega = \omega_c/N$, and the discrete frequency is $\omega_n = n\,\Delta\omega$. As can be observed from

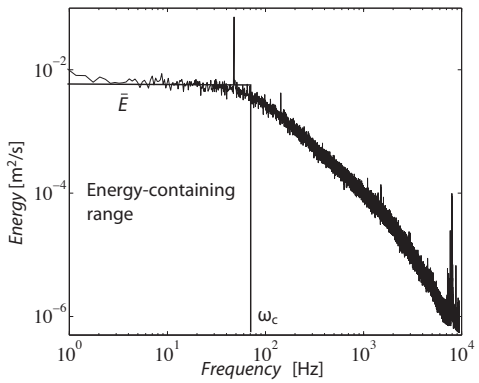

Figure 3. Energy spectrum of the air velocity measured within the diffuser of the spunbonding rig at x = 350 mm (see Part I).

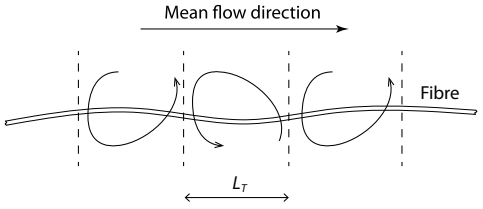

Figure 4. Schematic of a portion of fibre in a turbulent flow with integral length scale L_T.

the energy spectrum in the diffuser (Figure 3), a reasonable simplification is to consider only the low-frequency portion of the spectrum where the energy is constant up to a cut-off frequency ω_c

$$E(\omega) = \begin{cases} \bar{E} & 0 \le \omega \le \omega_c \\ 0 & \omega > \omega_c \end{cases} \tag{8}$$

Once ω_c is known the constant energy component $\bar{E}$ is obtained from the turbulent kinetic energy u^2 of the velocity signal by means of

$$u^2 = \langle u(t)^2 \rangle = \int_0^{+\infty} E(\omega)\, \mathrm{d}\omega \tag{9}$$

which leads to $u^2 = \bar{E}\,\omega_c$.

So far we considered only the time scale of the turbulent velocity in Equation 5 without mentioning how the signal varies in space. The integral time of turbulence, which is defined as the time lag necessary for two velocity data measured at one point to become uncorrelated, can be estimated from the velocity history as

$$T_I = \int_0^{\infty} \frac{R_U(\tau)}{R_U(0)}\, \mathrm{d}\tau \tag{10}$$

where $R_U(\tau)$ is the autocorrelation function of a single velocity time-history record

$$R_U(\tau) = \lim_{T\to\infty} \frac{1}{T} \int_0^T U(t)\, U(t+\tau)\, \mathrm{d}t \tag{11}$$

Once T_I is calculated by Equation 10 the length scale of the fibre-turbulence interaction can be defined through Taylor's hypothesis of frozen turbulence [24], which states that turbulent eddies are dragged by the mean air flow and therefore travel at the mean flow velocity. Under this assumption the turbulent length scale is $L_T = T_I\, \overline{U}$, which corresponds to the distance at which two air velocity signals are uncorrelated. Using this technique the turbulence length scale was measured in Part I, and it was shown that in the spun-bonding diffuser L_T is in the range 19 - 23 mm.

Figure 4 shows this picture for a fibre immersed in a turbulent air flow characterized by mean velocity $\overline{\boldsymbol{U}}$ and turbulence length scale L_T. In this formulation uncorrelated eddies interact with the fibre at intervals of L_T along the fibre length, which can be modelled as a turbulent air drag force that acts at regular intervals L_T along the fibre.

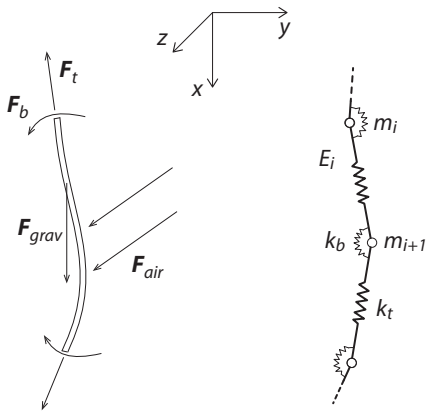

Figure 5. Schematic of a fibre subject to gravity and an air drag force (*left*), modelled as a series of beads connected by linear and rotational springs (*right*).

Model description

Fibre formulation

In the spunbonding process the fibre-air flow interaction can be divided into two steps. In the first stage, which takes place in the contraction, molten filaments are aligned with the accelerated air stream and solidify into fibres under a skin friction drag force. Then, in the diffuser, the increase of turbulence intensity produces random fibres oscillation with an amplitude that grows downstream in the diffuser. In this study we focus on the behaviour of a fibre in the diffuser.

In the model the fibre has length L, diameter d, and is discretised into N elements E_i with a length l equal to the turbulent length scale L_T characteristic of the turbulent flow, as shown in Figure 5. The mass of a fibre element E_i is $\Delta m = \rho_f l \pi d^2/4$, where ρ_f is the density of the fibre, and is concentrated at the element ends i and $i+1$. As a result the fibre is formed by a chain of $N+1$ beads with mass $m_i = \Delta m$ for $i = 2, \ldots, N$, and $m_i = \Delta m/2$ for $i = 1$ and $i = N+1$.

Dynamic equations of fibre motion

With reference to Figure 5 the position of the i-th bead is described by $\mathbf{r}_i = x_i\mathbf{i} + y_i\mathbf{j} + z_i\mathbf{k}$ where $\mathbf{i}, \mathbf{j}, \mathbf{k}$ are the unit vectors aligned with the Cartesian frame x, y, z. The fibre beads are subject to (1) an air drag force $\mathbf{F}_{\rm air}$, (2) a gravity force $\mathbf{F}_{\rm grav}$, as external forces, and (3) a tensile elastic force $\mathbf{F}_{\rm t}$, and (4) a bending elastic force $\mathbf{F}_{\rm b}$, as internal forces. The dynamic equations that govern the fibre motion are

$$m_i \frac{{\rm d}^2\mathbf{r}_i}{{\rm d}t^2} = \mathbf{F}_{{\rm air},i} + \mathbf{F}_{{\rm t},i} + \mathbf{F}_{{\rm b},i} + \mathbf{F}_{{\rm grav},i} \qquad (12)$$

In the simulations the fibre starts aligned with $\mathbf{i}$ and the gravity force at the ith bead is $\mathbf{F}_{{\rm grav},i} = m_i g\mathbf{i}$ where $g = 9.81$ m/s^2 is the gravity acceleration.

Air drag force

The air drag force is evaluated at the centre of a fibre element E_i in terms of the velocity of the air flow relative to the fibre element evaluated at the element centre of mass

$$\mathbf{V}_i = \mathbf{U}_i - \frac{1}{2}\left(\frac{{\rm d}\mathbf{r}_i}{{\rm d}t} + \frac{{\rm d}\mathbf{r}_{i+1}}{{\rm d}t}\right) \qquad (13)$$

where $\mathbf{U}_i$ is the air flow velocity obtained using Equations 5-6. To calculate the air drag force with Equations 1-4, is necessary to decompose the relative velocity $\mathbf{V}_i$ into two directions $\mathbf{t}_i$ and $\mathbf{n}_i$ respectively tangential and normal to the fibre axis, as shown in Figure 6. The tangential direction is defined as

$$\mathbf{t}_i = \frac{\mathbf{r}_{i+1} - \mathbf{r}_i}{|\mathbf{r}_{i+1} - \mathbf{r}_i|} \qquad (14)$$

while for the normal direction it is necessary first to define the plane that contains both the fibre axis and the air velocity

$$\mathbf{u}_i = \mathbf{t}_i \times \mathbf{V}_i \qquad (15)$$

then the normal direction is calculated as

$$\mathbf{n}_i = \frac{\mathbf{t}_i \times \mathbf{u}_i}{|\mathbf{t}_i \times \mathbf{u}_i|} \qquad (16)$$

It follows that the tangential and normal air velocity are

$$\mathbf{V}_{\rm t} = (\mathbf{V}\cdot\mathbf{t})\,\mathbf{t} \qquad (17)$$

$$\mathbf{V}_{\rm n} = (\mathbf{V}\cdot\mathbf{n})\,\mathbf{n} \qquad (18)$$

and the tangential skin friction force and the normal drag force from Equations 1-3 are

$$\mathbf{F}_{\rm t} = \frac{1}{2}\pi d l \rho_a C_f \mathbf{V}_{\rm t}^2 \mathbf{t} \qquad (19)$$

$$\mathbf{F}_{\rm n} = \frac{1}{2} d l \rho_a C_n \mathbf{V}_{\rm n}^2 \mathbf{n} \qquad (20)$$

where C_f is calculated using $\beta = 0.9$ for a single fibre in a tube[20]. The total drag force in the fibre element is $\mathbf{F} = \mathbf{F}_{\rm t} + \mathbf{F}_{\rm n}$ and, since each bead m_i shares two elements E_{i-1} and E_i, the air drag force acting on the i-th bead is

$$\mathbf{F}_{{\rm air},i} = \frac{1}{2}\left(\mathbf{F}_{i-1} + \mathbf{F}_i\right) \qquad (21)$$

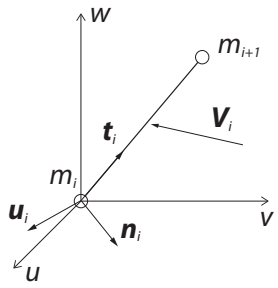

Figure 6. Fibre element subject to air flow velocity with the local frame where the air drag force is defined.

Tensile force

An internal elastic force that restores the initial length l of a fibre element along the tangential direction $\mathbf{t}$ is included in the model. This is modelled by a linear spring that

applies at the two ends of the fibre element a force which is proportional to the elongation of the element

$$f_{t,i} = k_b \left(|\mathbf{r}_{i+1} - \mathbf{r}_i| - l \right) \tag{22}$$

where the spring constant is

$$k_b = \frac{E\pi d^2}{4l} \tag{23}$$

and E is the Young modulus of the material. As a result the tangential force on the i-th bead is the sum of the contribution from the elements E_{i-1} and E_i

$$\mathbf{F}_{\mathrm{t},i} = -f_{t,i-1}\mathbf{t}_{i-1} + f_{t,i}\mathbf{t}_i \tag{24}$$

Bending force

From slender beam theory the curvature κ of the centreline of a beam is related to the applied bending moment M_b through

$$\kappa = \frac{M_b}{EI} \tag{25}$$

where the curvature is $\kappa = \mathrm{d}\theta/\mathrm{d}s$ and $\theta(s)$ is the orientation of the centreline. In the model the bending stiffness is modelled by a rotational spring at node i that applies a bending moment which is proportional to the misalignment of two adjacent fibre elements, namely

$$\mathbf{M}_i = -k_b \Delta\theta_i \mathbf{u}_{\mathrm{n},i} \tag{26}$$

where $k_b = EI/l$, $\mathbf{u}_{n,i}$ is the normal to the plane that contains the tangents vectors $\mathbf{t}_{i-1}$ and $\mathbf{t}_i$

$$\mathbf{u}_{\mathrm{n},i} = \frac{\mathbf{t}_{i-1} \times \mathbf{t}_i}{\|\mathbf{t}_{i-1} \times \mathbf{t}_i\|} \tag{27}$$

and the misalignment between adjacent fibre elements is

$$\Delta\theta_i = \frac{\mathbf{t}_{i-1} \cdot \mathbf{t}_i}{\|\mathbf{t}_{i-1}\| \|\mathbf{t}_i\|} \tag{28}$$

In the lumped mass formulation the rotational dynamic equations are suppressed and moments are converted into forces applied at the node positions. From beam theory the bending moment is related to the shear force by $S = \mathrm{d}M/\mathrm{d}s$. Following a similar approach to van den Boom et al.[25] the discrete shear forces on the fibre elements are

$$\mathbf{S}_{i-1} = (M_i \mathbf{u}_{\mathrm{b},i}^{(i-1)} - M_{i-1}\mathbf{u}_{\mathrm{b},i-1}^{(i-1)})/l \tag{29}$$

$$\mathbf{S}_i = (M_{i+1}\mathbf{u}_{\mathrm{b},i+1}^{(i)} - M_i \mathbf{u}_{\mathrm{b},i}^{(i)})/l \tag{30}$$

where the bi-normal vector

$$\mathbf{u}_{\mathrm{b},i}^{(j)} = \mathbf{u}_{\mathrm{n},i} \times \mathbf{t}_j \tag{31}$$

defines the direction of the shear force applied to element j by the bending moment at node i, as shown in Figure 7. The force component acting on the i-th node is obtained from the shear force vectors on adjacent elements:

$$\mathbf{F}_{b,i} = \mathbf{S}_{i-1} - \mathbf{S}_i \tag{32}$$

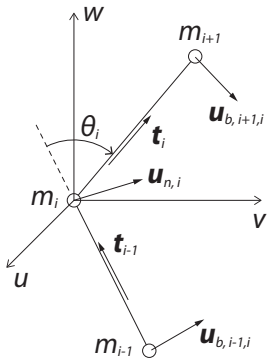

Figure 7. Schematic of two adjacent fibre elements and the unit vectors used for the bending forces definition.

Accuracy and convergence of dynamic simulations

Dynamic simulations of fibre motion in a turbulent flow were undertaken by integrating Equation 12 in the time interval [0, 1 s] using a semi-implicit Euler scheme and the parameters listed in Table 1. The energy of turbulence is given by the non-dimensional turbulent intensity Tu, which represents the ratio between the rms u and the mean velocity U. The boundary conditions were $\mathbf{r}_1 = (0\,0\,0)^T$, at the first node, and a free end boundary condition at the end node, to reproduce the configuration of the experiments in Part I.

The accuracy of an explicit integration scheme strongly depends on the length of time step h; in particular if the solution has an oscillatory behaviour it is necessary to use very small time steps[26]. A solution that is often adopted is to include physical damping in the model to reduce the amplitude of the oscillations. This however has two drawbacks: it modifies the natural dynamic solution if the system is over damped, and it requires even smaller time steps to reach a stable solution[27]. Therefore, it was decided to exclude damping from the governing dynamics of the fibre.

According to the theorem of energy of a dynamical system[28] the kinetic energy of the system is equal to the work done by the applied forces. This equality was used to verify the accuracy and convergence of a simulation through the difference between the total work done on the masses and kinetic energy of the fibre during the simulation. The kinetic energy of the fibre at time t_k is

$$T(t_k) = \sum_{i=1}^{N} \frac{1}{2} m_i \|\mathbf{v}_{k,i}\|^2 \tag{33}$$

where $\mathbf{v}_{k,i} = \mathbf{v}_i(t_k)$ is the instantaneous velocity of the i-th bead. The work done on the fibre is given by the sum of the contribution on each bead. By definition the work done on the i-th bead that moves along the path Γ as a results of the applied force $\mathbf{F}_i$ is

$$W_i = \int_\Gamma \mathbf{F}_i \cdot \mathrm{d}\mathbf{r}_i \tag{34}$$

where $\mathbf{F}_i$ is the total force on bead i. During the simulation, the work at time t_k can be evaluated through the trapezoidal

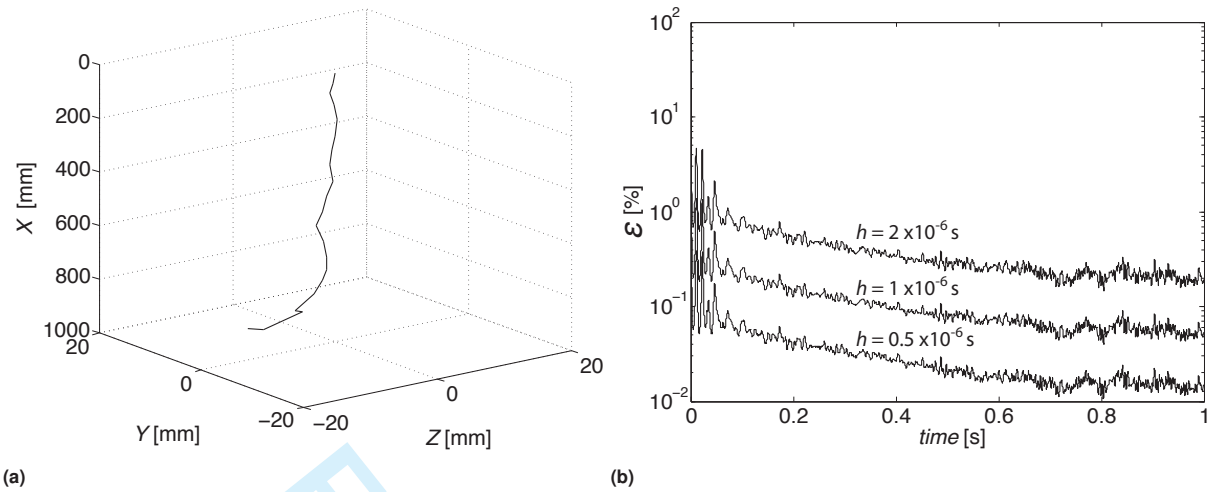

Figure 8. Accuracy of the model, (a) fibre at the end of the simulation and (b) evolution of the error ε for three different time steps. Note the magnification along the X-Z axes in (a)

Table 1. Parameters used for the simulations

d (μm)	U (m/s)	Tu (-)	L_T (mm)	f (Hz)	E (GPa)	ρ_f (kg/m^3)
50	10	0.1	50	100	2	950

rule as

$$W(t_k)_i = \sum_{j=1}^{k-1} \frac{1}{2} \left(\mathbf{F}_{j,i} + \mathbf{F}_{j+1,i}\right) \cdot \left(\mathbf{r}_{j+1,i} - \mathbf{r}_{j,i}\right) \quad (35)$$

and the total work on the fibre is obtained as the sum over the N beads.

Figure 8a shows the profile of the fibre at the end of a simulation carried out in Matlab R2012a using a time step $h = 10^{-6}$ s, which required 2.7 hours of CPU time on an Intel 1.97 GHz, 3.25 GB of RAM. The evolution of the error

$$\varepsilon_k = \frac{|W_k - T_k|}{T_k} \times 100 \quad (36)$$

is presented for three different time steps in Figure 8b. This demonstrates the good stability of the model, and that the accuracy of the simulation increases by decreasing the time step, as shown by the tendency of ε to offset towards lower error values for smaller time steps. Since decreasing the time step increases the CPU time proportionally, the simulations presented in the next section were carried with a time step $h = 10^{-6}$ s, which correspond to an error of less than 1%.

Fibre behaviour in turbulent flows

In Part I the amplitude of motion of a filament with diameter 200 μm and a fibre with diameter 18 μm were measured in a spunbonding diffuser. In this section we extend the investigation numerically, using the fibre model to predict the amplitude and frequency of fibre oscillation as a function of the measured air flow parameters and the fibre diameter. The effect of mean air velocity, turbulent intensity, frequency of turbulence, fibre diameter, and turbulent length scale was studied by varying individually the parameters listed in Table 1, for a fibre of length 1 metre. The turbulent drag force was calculated using the air velocity components along the x, y and z directions independently generated using Equations 5-6.

The random fibre oscillatory motion was characterised in terms of the end node position $\mathbf{r}(t)_{N+1}$. The amplitude of motion was measured by the standard deviation of the displacement along the y and z directions, and the frequency of the random oscillations as the number of times the node crosses the planes $x - z$ and $x - y$ divided by 2^{15}. All the results are presented as mean values calculated over ten simulations obtained with different turbulent air velocity histories.

Figure 9 shows that both the amplitude and the frequency of the fibre motion grow almost linearly with the mean air velocity, due to the increased air drag force acting on the fibre. A similar behaviour is observed also when the fluctuating turbulent velocity is increased, as shown in Figure 10. In this case however, the frequency of oscillation increases until $Tu = 0.15$ and then is nearly constant. The results for the amplitude are in line with the observation for the single fibre in Part I, although in the simulations the mean and the fluctuating air velocity are varied independently, whereas in the spun-bonding diffuser they are connected.

The fibre diameter has a twofold effect on the behaviour of the fibre. By increasing the diameter of the fibre the area of the elements exposed to the air flow increases, so increasing the air drag force. However, as the fibre diameter grows, the inertia and the gravity force become progressively more significant, and the amplitude of oscillation is reduced. This explains the sigmoidal shape of the plot in Figure 11a. Again, the results are in agreement with the measurement in Part I, where the amplitude of motion for the filament with diameter 200 μm is bigger than the amplitude of motion for the fibre

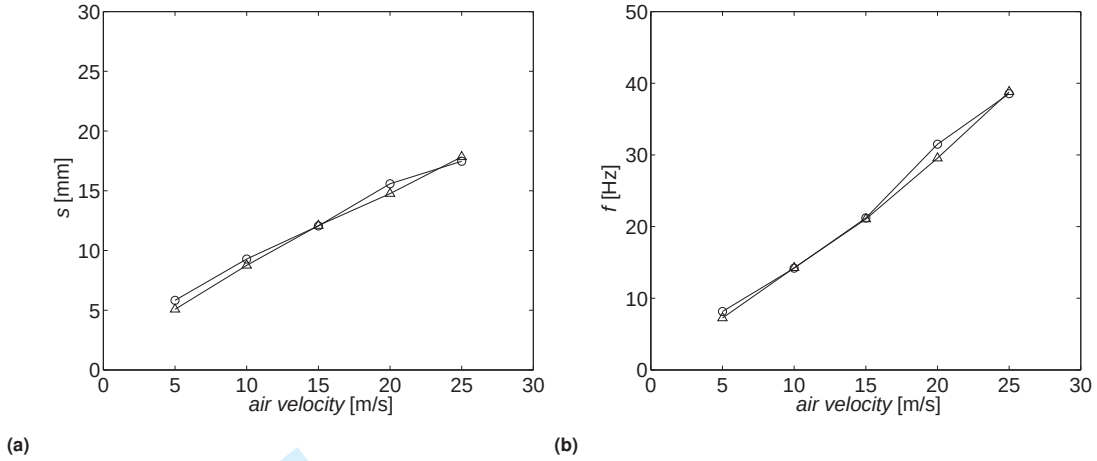

Figure 9. Role of the mean air velocity in the fibre dynamics: (a) standard deviation of the end node motion, and (b) frequency of oscillation of the end node, along the y direction (circles) and the z direction (triangles).

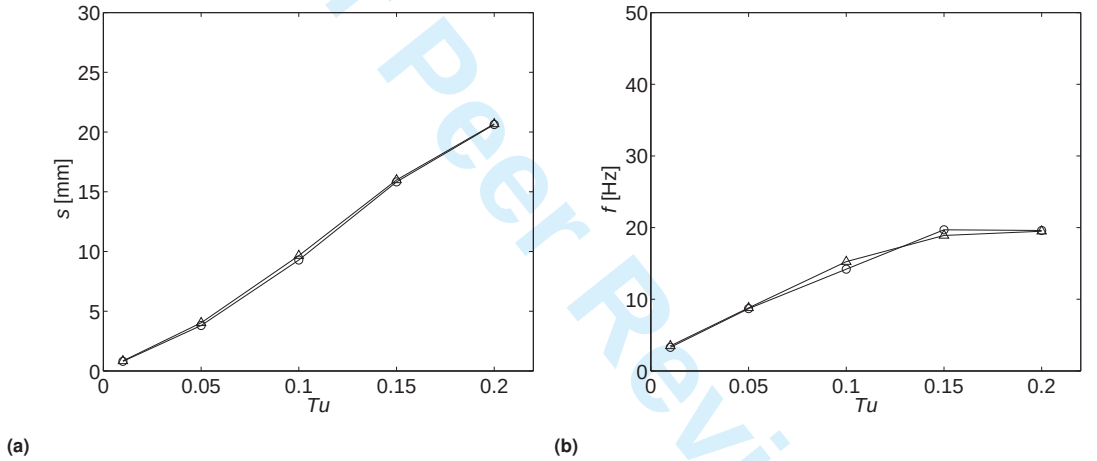

Figure 10. Role of the turbulent intensity in the fibre dynamics: (a) standard deviation, and (b) frequency of oscillation of the end node, along the y direction (circles) and the z direction (triangles).

with diameter 18 μm.

The turbulent length scale L_T represents an estimate of the interval at which turbulent drag forces are uncorrelated along the fibre. Figure 11b shows that, as the turbulent length scale L_T increases, the amplitude of fibre motion increases. Note that by increasing L_T the number of fibre elements decreases, and a reduced fibre displacement could be expected as a result of apparent geometrical stiffness[9]. However, due to tensile force applied by the air flow, the fibre is mainly straightened along the mean flow direction, which confirms the results of the model and the validity of our turbulent force formulation.

Figure 11c shows the effect of varying the cut-off frequency in the energy spectrum, while keeping constant the total energy, i.e. for a constant value of the turbulent velocity u. The amplitude of fibre motion strongly decreases when increasing the frequency of turbulence. This is in line with the expected role of the the turbulent length scale, as decreasing L_T is equivalent to increasing the spatial frequency of turbulence.

Concluding discussion

Fibre dynamics in turbulent flows

In the spun-bonding process the fibre web develops during the laydown as a result of the fibre motion at the exit of the diffuser and the interaction with the conveyor belt. In the companion paper, Part I, it was observed that before deposition the fibres oscillate randomly with an amplitude of motion that depends on parameters of the air flow in the diffuser, and on the diameter of the fibre.

In this paper, Part II, we presented a three-dimensional model that simulates the dynamics of fibres in turbulent flows. The model guarantees good accuracy and stability which allows for applications in nonwoven textiles fibres, where the large magnitude and frequency of oscillation of

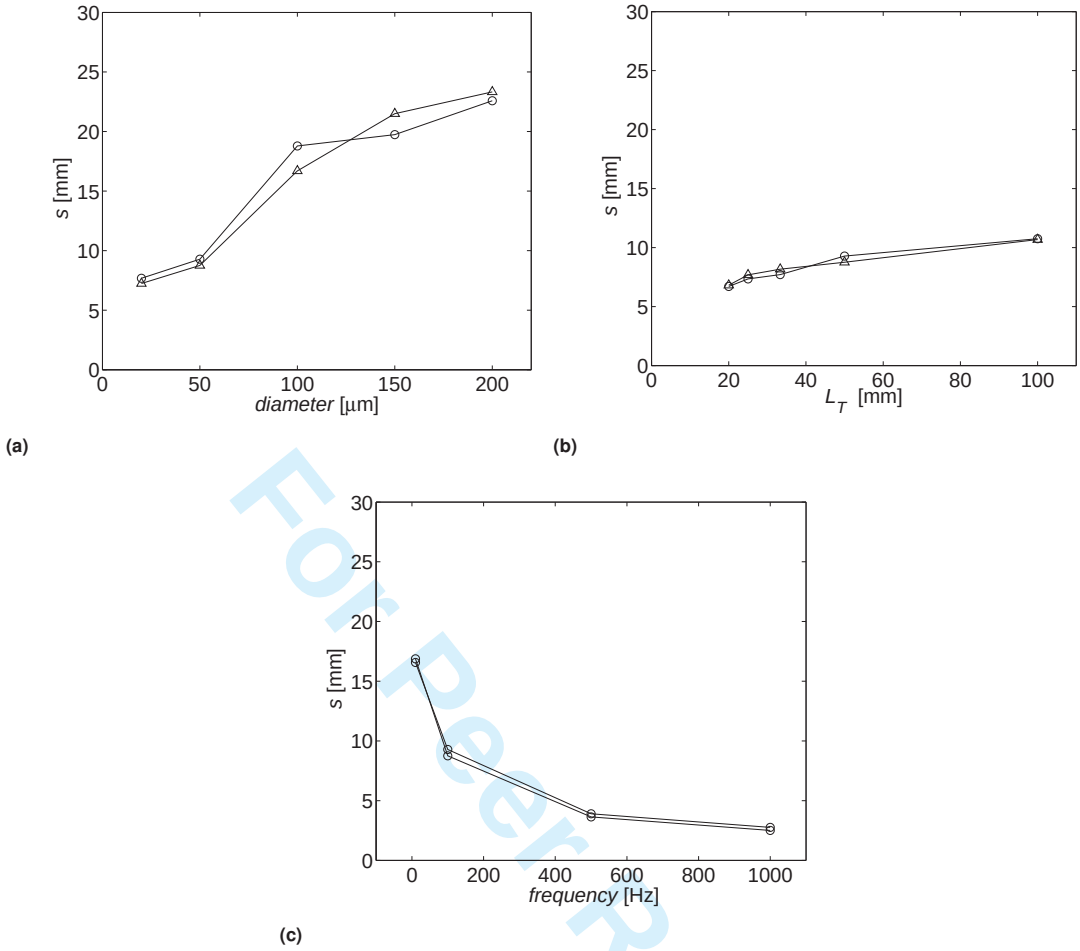

Figure 11. Standard deviation of oscillation of the end node, along the y direction (circles) and the z direction (triangles), as a function of (a) the fibre diameter, (b) the turbulent length scale, and (c) the frequency of turbulence.

the air drag, compared to the low inertia of the fibre, make it difficult to obtain realistic numerical simulations.

The amplitude and frequency of fibre oscillation have been studied at the free end of the fibre, as a function of the measured air flow parameters. The amplitude of fibre motion increases with the mean air flow velocity, the turbulent intensity, the fibre diameter, and the turbulent length scale, whereas it decreases with the frequency of turbulence. The results for the flow velocity and fibre diameter agree qualitatively with those measured in the first part of this paper, and are a crucial prerequisite for understanding the development of the fibre geometry during deposition.

Fibre laydown and future work

The coiling of ropes laying on to a horizontal plane has been studied both mathematically and experimentally. Mahadeven[29] showed numerically that the coiling radius of the rope is a function of the feeding velocity, the stiffness, and the density of the rope. Previously Hearle[30–32] found in his experiments that a thread which is laid on to a moving belt assumes the form of a modified cycloid whose shape is a function of the feeding height, the elasticity of the thread, and the velocity of the belt. Unfortunately, it is not possible to translate directly these results to the laydown of nonwoven fibres due to the predominant effect that the air drag force has over the fibre stiffness, and the effect of the air suction towards the conveyor belt that affects the fibre-belt contact forces. However, there is no doubt that the oscillation of the fibre that exits the diffuser is directly related to the motion of the fibre point of deposition, and that this determines the geometry of the web. In the spunbonding process turbulence is used to enhance the fibre motion and increase the isotropy of fibre orientation in the web, but if the intensity of turbulence is too high then the areal density of the web becomes progressively less uniform and the quality of the material is compromised.

A full investigation of the web formation requires a detailed study of the fibre laydown which combines fibre motion with the fibre coiling and the effect of the fibre-belt contact. This paper and its companion, Part I, have shown how the fibre displacement is influenced by the fibre diameter and the parameters of the air flow. Further air flow measurements and computational fluid dynamics simulations are necessary for

a better understanding of how to control these parameters in the spunbonding process, these topics are beyond the scope of this paper. A detailed dynamic model for the fibre laydown is under development, which will use the result of amplitude and frequency of fibre motion outlined in this work to study the pattern of fibres laying on to the web[33].

Acknowledgements

The authors are grateful to Fitesa Germany GmbH for the financial support.

References

1. Beyreuther R and Brunig H. *Dynamics of fibre formation and processing*. Berlin: Springer, 2010.
2. Bhat G S and Malkan S R. Extruded continuous filament nonwovens: Advances in scientific aspects. *J Appl Polym Sci* 2002; 83(3):572–585.
3. Battocchio F and Sutcliffe M P F. Fibre behaviour in the spunbonding process. Part I: Characterisation of air flow and fibre motion. *submitted to: Proc Inst Mech Eng C J Mech Eng Sci*, 2015.
4. Bo Z. Experimental study and numerical analysis for prediction of the fibre diameter of polylactic acid (PLA) spunbonded nonwovens. *Fibres Text East Eur* 2009; 76(5):82–86.
5. Zhao B. Effects of processing parameters on the filament fiber diameter of spunbonded nonwoven fabrics. *Polym Eng Sci* 2007; 47(4):510–515.
6. Yamamoto S and Matsuoka T. A method for dynamic simulation of rigid and flexible fibers in a flow field. *J Chem Phys* 1993; 98(1):644–650.
7. Nyland G H and Skjetne P and Mikkelsen A and Elgsaeter A. Brownian dynamics simulation of needle chains. *J Chem Phys* 1996; 105(3):1198–1207.
8. Ross R F and Klingenberg D J. Dynamic simulation of flexible fibers composed of linked rigid bodies. *J Chem Phys* 1997; 106(7):2949–2960.
9. Wang G and Yu W. and Zhou C. Optimization of the rod chain model to simulate the motions of a long flexible fiber in simple shear flows. *Eur J Mech B-Fluid* 2006; 25(3):337–347.
10. Xiang P and Kuznetsov A V. Simulation of shape dynamics of a long flexible fiber in a turbulent flow in the hydroentanglement process. *Int Comm Heat Mass* 2008; 35(5):529–534.
11. Hadap S and Magnenat-Thalmann N. Modeling dynamic hair as a continuum. *Comput Graph Forum* 2001; 20(3):329–338.
12. Featherstone R (2008) *Rigid body dynamics algorithm*. Springer.
13. Featherstone R. An empirical study of the joint space inertia matrix. *Comput Graph Forum* 2004; 23(9):859–871.
14. Rao R S and Shambaugh R L. Vibration and stability in the melt blowing process. *Ind Eng Chem* 1993; 32(12):3100–3111.
15. Marla V T and Shambaugh R L. Three-dimensional model of the melt-blowing process. *Ind Eng Chem* 2003; 42(26):6993–7005.
16. Sun Y and Zeng Y and Wang X. Three-dimensional model of whipping motion in the processing of microfibers. *Ind Eng Chem* 2011; 50(2):1099–1109.
17. Sakiadis B C. Boundary-layer behavior on continuous solid surfaces: III. The boundary layer on a continuous cylindrical surface *AIChE J* 1961; 7(3):467–472.
18. Matsui M. Air drag on a continuous filament in melt spinning *T Soc Rheol* 1976; 20(3):465–473.
19. Ju Y D and Shambaugh R L. Air drag on fine filaments at oblique and normal angles to the air stream *Polym Eng Sci* 1994; 34(12):958–964.
20. Majumdar B and Shambaugh R L. Air drag on filaments in the melt blowing process *J Rheol* 1990; 34(4):591–601.
21. Newland E D. *An Introduction to random vibrations, spectral and wavelet analysis*. Longman Scientific and Technical, 1993.
22. Pope S B. *Turbulent flows*. Cambridge University Press, 2000.
23. Shinozuka M and Deodatis G. Simulation of stochastic processes by spectral representation *Appl Mech Rev* 1991; 44(4):191–203.
24. Taylor G I. The spectrum of turbulence *Proc R Soc A* 1938; 164:479–490.
25. van den Boom H J J and Dekker J N and van Elsacker A W. Dynamic aspects of offshore riser and mooring concepts *Proceedings of the Offshore Technology Conference, 27-30 April 1987, Houston, Texas*
26. Moin P. *Fundamentals of engineering numerical analysis*. Cambridge University Press, 2010
27. *ABAQUS/CAE 6.9 User's manual*. Hibbit, Karlsson & Sorensen Inc., 2002
28. Goldstein H and Poole C P. (2001) *Classical Mechanics*. Addison-Wesley.
29. Mahadevan L and Keller J B. Coiling of flexible ropes *Proc R Soc A* 1996; 452:1679–1694.
30. Hearle J W S and Sultan M A I and Govender S. Form taken by threads laid on a moving belt - I. Experimental study *J Text I* 1976; 67(11):373–376.
31. Hearle J W S and Sultan M A I and Govender S. Form taken by threads laid on a moving belt - II. Mechanisms and theory *J Text I* 1976; 67(11):377–381.
32. Hearle J W S and Sultan M A I and Govender S. Form taken by threads laid on a moving belt - III. Comparison of materials *J Text I* 1976; 67(11):382–386.
33. Battocchio F. *Manufacture and characterisation of spunbonded nonwovens*. PhD thesis, University of Cambridge, UK, 2014.